

Active nonreciprocal attraction between motile particles in an elastic medium

Rahul Kumar Gupta¹, Raushan Kant², Harsh Soni², A.K. Sood² and Sriram Ramaswamy²

¹Tata Institute of Fundamental Research, Gopanpally, Hyderabad 500 107 India and

²Department of Physics, Indian Institute of Science, Bangalore 560 012, India

(Dated: August 10, 2020)

We present a theory for the interaction between motile particles in an elastic medium on a substrate, relying on two arguments: a moving particle creates a conspicuously fore-aft asymmetric distortion in the the elastic medium; this strain field reorients other particles. We show that this leads to sensing, attraction and pursuit, with a non-reciprocal character, between a pair of motile particles. We confirm the predicted distortion fields and non-mutual trail-following in our experiments and simulations on polar granular rods made motile by vibration, moving through a dense monolayer of beads in its crystalline phase. Our theory should be of relevance to the interaction of motile cells in the extracellular matrix or in a supported layer of gel or tissue.

A self-propelled particle moving through a fluid medium influences other such particles through an interaction that is long-ranged in the purely viscous limit, with profound consequences for pair dynamics and collective behaviour [1–5]. In an ordered medium at thermal equilibrium, dispersed particles interact through long-ranged structural distortions [6], suppression of fluctuations, [7, 8], or sharing a disordered wetting layer [9]. When the medium is held far from equilibrium novel fluctuation forces arise between inclusions [10, 11]. The case of living cells, interacting through the distortions that their intrinsic active force-dipoles produce in an elastic medium such as the extracellular matrix, has received considerable attention [12–17]. The treatment, however, is primarily in terms of an effective interaction energy, and moreover does not take into account the motility of the cells. Active polar order in elastic media has been studied in [18–24], with a fully rotation-invariant theory in [25]. Henkes et al. [26] study the effect of a collection of motile but non-interacting active Brownian particles on an elastic medium on a substrate.

In this Letter we construct the single-particle and pair dynamics of geometrically polar active objects in a damped elastic medium, and present evidence supporting our predictions from laboratory and numerical experiments. Our detailed results are for dimension $d = 2$ but their general structure applies to $d = 3$ as well [27]. We show that the force monopole carried by a single self-propelled rod with speed v_0 gives rise to an elastic wake with anisotropic screening beyond length scales $\xi \equiv \mu/\zeta v_0$ where μ is a typical elastic modulus of the medium and ζ a damping coefficient. The exponential screening is strongest ahead of the rod and absent directly behind it. The lattice distortions produced by a given rod reorient other rods, thus presenting an explicit mechanical realization of an active non-reciprocal interaction [28–37] between pairs of rods that cannot be described in terms of a potential energy. We test our theory in simulations and experiments on monolayers of vibrated grains. We find confirmation of the form of the single-particle elastic field (Fig. 1), and of the non-reciprocal

character of the pair interaction in the form of pursuit-and-capture events (Fig.4).

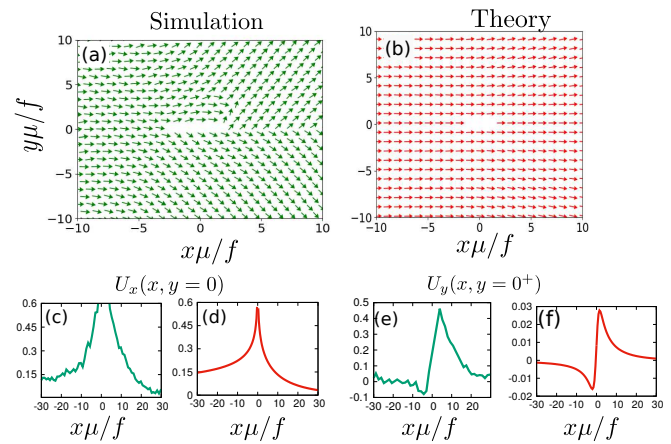


FIG. 1. Unit vector profile of the displacement field: (a) around a moving rod in the crystalline bead medium from the simulation, and (b) around a force monopole moving along the x direction calculated from the theory. (c) & (d) x dependence of U_x at $y = 0$ in simulation and theory: both cases see the rapid decay of $U_x(x, y = 0)$ for $x > 0$ as compared to $x < 0$. (e) & (f) x dependence of U_y at $y\mu/f = 1.8$ in simulation and theory. In simulation, $\phi_b = 0.80$ and $f/\mu = 2.2a$.

We now show how we arrived at these findings. We begin with the calculation of the Eulerian displacement field $\mathbf{u}(\mathbf{x}, t)$ of an elastic medium on a substrate, driven by a single motile polar particle. Unlike in [26], we distinguish the particles driving the medium from those that comprise it, and in the present work our focus is on single-particle and pair dynamics, not collective behaviour. We do not offer a theory of the motility of the particle but simply assume its position $\mathbf{R}(t)$ follows

$$\dot{\mathbf{R}}(t) = v_0 \mathbf{n}(t) \quad (1)$$

where the unit vector $\mathbf{n}(t)$ is its orientation at time t and the speed v_0 is assumed to be fixed by the motility mechanism. It is straightforward to include noise in (1)

as well as in the dynamics of $\mathbf{n}(t)$ and the medium, but our analysis will focus on the deterministic part of the dynamics.

We assume that in the absence of driving $\mathbf{u}(\mathbf{x}, t)$ is governed by a free energy functional

$$F = \int d^2x [\lambda(\text{Tr}\boldsymbol{\varepsilon})^2/2 + \mu\text{Tr}(\boldsymbol{\varepsilon}^2)] \quad (2)$$

where $\boldsymbol{\varepsilon} = (\nabla\mathbf{u} + \nabla\mathbf{u}^T)/2$ is the symmetric strain tensor [38]. We treat the medium as an isotropic elastic continuum, ignoring for now the role of preferred directions in the lattice [39]. Indeed, our treatment does not assume a crystalline medium, merely one with a shear and a bulk modulus, and as such should apply to motion through a glass or gel, modulo effects of quenched disorder. As argued in [40], the pushing or dragging of the beads by the motile rod amounts to a point force density $f\delta(\mathbf{r} - \mathbf{R}(t))\mathbf{n}(t)$ at the location of the rod. Such a monopole of force, proportional to the local polarization, is permitted because the system is in contact with a substrate which serves as a momentum sink [25, 40–42]. We will treat v_0 and f as independent phenomenological parameters, although they must be related by the detailed mechanics of our system. The equation of motion for \mathbf{u} for zero inertia then reads

$$\zeta\partial_t\mathbf{u} = -\frac{\delta F}{\delta\mathbf{u}} + f\delta(\mathbf{r} - \mathbf{R}(t))\mathbf{n}(t), \quad (3)$$

as in [26] except that the forcing is by a single active particle. Here ζ is the coefficient of drag on the elastic medium due to the substrate. Let the displacement field in a frame comoving and co-rotating with the rod be \mathbf{U} , which is stationary if no other moving rods are present. The lab-frame displacement $\mathbf{u}(\mathbf{r}, t) = \mathbf{S}(t) \cdot \mathbf{U}(\mathbf{r}')$, where \mathbf{S} is the rotation matrix from the frame fixed in the rod to the lab frame and $\mathbf{r}' = \mathbf{S}^T \cdot (\mathbf{r} - \mathbf{R}(t))$. For the case where the motile particle points and moves along $\hat{\mathbf{x}}$, Eq. (3) simplifies ([43], S1) to

$$[-\zeta v_0\partial_x - (\mu\nabla^2 + \lambda\nabla\nabla\cdot)]\mathbf{U} = f\delta(\mathbf{r})\hat{\mathbf{x}}. \quad (4)$$

Solving (4) in Fourier space and inverting [44] gives the x and y components of \mathbf{U} ([43], S1):

$$U_x = \frac{f}{4\pi\mu} \left\{ \left[K_0\left(\frac{r}{2\xi}\right) - \frac{x}{r} K_1\left(\frac{r}{2\xi}\right) \right] e^{-\frac{x}{2\xi}} \right. \quad (5)$$

$$\left. + \nu \left[K_0\left(\frac{\nu r}{2\xi}\right) + \frac{x}{r} K_1\left(\frac{\nu r}{2\xi}\right) \right] e^{-\frac{\nu x}{2\xi}} \right\}$$

$$U_y = \frac{f}{4\pi\mu r} \left[\nu K_1\left(\frac{\nu r}{2\xi}\right) e^{-\frac{\nu x}{2\xi}} - K_1\left(\frac{r}{2\xi}\right) e^{-\frac{x}{2\xi}} \right] \quad (6)$$

where $r = \sqrt{x^2 + y^2}$, $\xi = \mu/\zeta v_0$ is a screening length, $\nu = (1+\eta)^{-1}$ with $\eta = \lambda/\mu$, and K_0 and K_1 are the modified Bessel functions of the second kind whose asymptotic

properties reveal that, for locations along the x axis, the dominant large- x decay of \mathbf{U} is exponential ahead of the motile particle but only as $1/\sqrt{x}$ behind it [see Fig. 1(d) and (f)]. We will see below that this extreme asymmetry confers stealth on a motile rod as it approaches another from behind, a feature central to the non-reciprocal pair interaction.

Note from (4) that the force monopole introduces a quantity f/μ with units of length [45]. It is thus useful to define the dimensionless inverse screening length $\alpha = f/\mu\xi = \zeta f v_0 / \mu^2$, which can be viewed as a Péclet number comparing the time scales of diffusion of \mathbf{u} and directed motion of the motile particle for a distance f/μ . The unit vector profile of \mathbf{U} is shown in Fig. 1b for $\eta = 1.3$ and $\alpha = 0.1$.

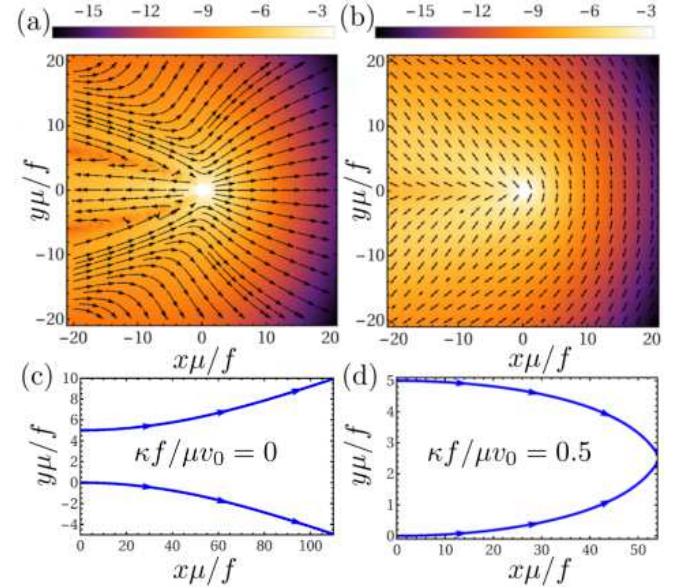


FIG. 2. For a single motile particle moving along the x direction: (a) Streamline plot of $\gamma_1\nabla^2\mathbf{u} + \gamma_2\nabla\mathbf{u}\cdot\mathbf{u}$ superimposed with the color map of its magnitude, and (b) Principal axis of the traceless part of $\kappa\boldsymbol{\varepsilon}$ superimposed with the color map of its positive eigen value at $\kappa f/\mu v_0 = 1$. The color map is shown on a log scale in both the figures. Trajectories of the two motile particles coupled with each other's displacement field via Eq. (7) for initial lateral distance $d\mu/f = 5$: (c) $\kappa f/\mu v_0 = 0$, and (d) $\kappa f/\mu v_0 = 0.5$. Here, $\gamma_1/v_0 = \gamma_2/v_0 = 1$, $\eta = 1$ and $\alpha = 1$.

In (1) we have ignored direct coupling of the particle to elastic distortions of the medium, and consequent interactions between inclusions [6]. We will see later that this neglect is wholly justified for the particles in our experiments and simulations. The effect of the elastic medium on a motile rod in our theory must therefore take place purely through rotation of \mathbf{n} and the resulting re-direction of the velocity of self-propulsion, much as in the imitation of chemotaxis by active colloids [33, 46–49]. The general form of the interaction of the orientation \mathbf{n}

with lattice distortions, as permitted by symmetry and at leading orders in gradients, is

$$\frac{d\mathbf{n}}{dt} = (\mathbf{I} - \mathbf{n}\mathbf{n}) \cdot [\kappa\boldsymbol{\varepsilon} \cdot \mathbf{n} + (\gamma_1 \nabla^2 + \gamma_2 \boldsymbol{\nabla} \boldsymbol{\nabla} \cdot) \mathbf{u}] . \quad (7)$$

The couplings in (7) could arise through an interaction free-energy $-(\kappa/2)\mathbf{n} \cdot \boldsymbol{\varepsilon} \cdot \mathbf{n} - \mathbf{n} \cdot (\gamma_1 \nabla^2 + \gamma_2 \boldsymbol{\nabla} \boldsymbol{\nabla} \cdot) \mathbf{u}$, with \mathbf{u} and $\boldsymbol{\varepsilon}$ evaluated at the position $\mathbf{R}(t)$ of the motile particle, or via active response to structural distortions [50]. In a gradient expansion, the phenomenological coefficient κ governs the leading apolar coupling, even under $\mathbf{n} \rightarrow -\mathbf{n}$, promoting the alignment of the axis of the particle along a principal direction of $\boldsymbol{\varepsilon}$. The γ_1, γ_2 terms, at next order in gradients and thus neglected in the related theory of oriented active solids [25], are nonetheless the leading *polar* coupling [19, 51], odd under $\mathbf{n} \rightarrow -\mathbf{n}$, biasing \mathbf{n} to point in a direction defined by a weighted average of the curvatures $\nabla^2 \mathbf{u}$ and $\boldsymbol{\nabla} \boldsymbol{\nabla} \cdot \mathbf{u}$. Such couplings entering through an energy function would of course lead to additional terms in (3), proportional to $\mathbf{n} \nabla \nabla \delta(\mathbf{r} - \mathbf{R}(t))$, but these would be subdominant in gradients relative to the f term so we ignore them. For a discussion on origins of γ_1, γ_2 see ([43], S2). To understand the behaviour implied by (7), we construct the streamline plot of $\gamma_1 \nabla^2 \mathbf{u} + \gamma_2 \boldsymbol{\nabla} \boldsymbol{\nabla} \cdot \mathbf{u}$ and the profile of the larger eigenvector of the traceless part of $\kappa\boldsymbol{\varepsilon}$, respectively, as created by a motile particle pointing along the x direction, choosing positive values for the relevant dimensionless combinations: $\gamma_1/v_0 = \gamma_2/v_0 = 1$, $\eta = 1$, $\kappa f/\mu v_0 = 1$ and $\alpha = 1$ (see Fig. 2a & b). Another motile particle placed in its vicinity will face torques tending to align it with the streamlines as in Fig. 2a, and to orient its axis along the extensional direction of $\boldsymbol{\varepsilon}$ as in Fig. 2b. The log-scale color maps in Fig. 2a & b show the rapid decay of strains and curvatures in the forward direction as mentioned above.

We now turn to the coupled dynamics of two motile particles ([43], S1), focusing on the simplest case of a pair initially oriented along the x direction with the same x coordinate, and separation d in the y direction. In order to calculate the threshold value of κ above which the particles attract each other, we substitute the value of the displacement field from Eq (5) in Eq. (7) and set $d\mathbf{n}/dt$ to zero with $n_x = 1$ and $n_y = 0$. We find that the motile particles turn so as to move towards each other above a critical value of κ , $\kappa_c f/\mu v_0 = \nu \alpha [\gamma_1/v_0 + \gamma_2/v_0 - (\gamma_1/v_0) \nu^{-3} K_1(d/2\xi)/K_1(\nu d/2\xi)]$. Fig. 2c & d show that the trajectories of two motile particles diverge at $\kappa = 0$ and converge at $\kappa f/\mu v_0 = 0.5$, respectively, for $d\mu/f = 5$, $\gamma_1/v_0 = \gamma_2/v_0 = 1$, $\eta = 1$ and $\alpha = 1$; here, $\kappa_c f/\mu v_0 = 0.26$.

We test our theory in experiments, and in simulations that re-create the experiments in a mechanically faithful manner and should therefore be viewed as numerical experiments. We work with a now well-established model active-matter system [40, 52, 53]: brass rods, 4.5 mm

long and tapered towards one end and hence geometrically polar, surrounded by aluminium beads of radius $a = 0.4$ mm, all confined between a pair of plates of fixed separation slightly larger than $2a$, agitated vertically, rendering the rods motile. Simulation and experimental details are provided in ([43], S5) and in [40, 54]. We chose this system because the bead medium flows like a fluid at low bead area fraction ϕ_b ($\lesssim 0.72$), but forms a crystalline lattice at high ϕ_b ([43], S6). As illustrated in Fig. 3a, at $\phi_b = 0.70$ the flow profile around a single rod has the two-lobed form expected for a monopole force density [40, 55] in a fluid on a substrate, whereas at high ϕ_b the flow is totally suppressed apart from a weak random component (see Fig. 3b and Supplementary Fig. 4 [43]). Crystal elasticity shuts down large-scale flow but the polar rod remains motile.

The first confirmation of our theory is seen in Fig. 1a & b. We see that the lattice displacement field around a single rod from the simulation at $\phi_b = 0.80$ qualitatively matches that predicted by our theory with $\eta = 1.3$ and $\alpha = 0.1$, except close to the polar rod whose nonzero size is not included in our theory (see [43], S3, for the details of the displacement field calculation). More convincingly, key predicted features of U_x (Fig. 1c & d) and U_y (Fig. 1e & f), including the rapid (slow) decay at positive (negative) x , and the distinctive profile of U_y , including its negative sign for $x < 0$, are well confirmed by the simulation, as are all qualitative features of the y dependence, (Supplementary Fig. 1, [43]). The x and y dependence of U_x are described satisfactorily by a common value of the parameters in (5) (Supplementary Fig. 1, [43]). Measured values of U_y exceed our theoretical estimates, for which we discuss possible reasons in the SI.

We now study the dynamics of two parallel rods initially pointing in the x direction. The initial longitudinal (x) distance between the rods is set to zero in all the experiments and simulations, at $\phi_b = 0.70$ and $d_0 = 15a$, the lateral distance $d(t)$ between the rods increases with time in both experiment and simulation (see Supplementary Movie S3, S4 and Supplementary Fig. 5a & b [43]). This is a simple consequence of the rotation of the orientation of each rod by the vortex generated by the other when the bead medium is fluid-like, at $\phi_b = 0.70$. Crucially, in the crystalline medium, the rods attract each other as shown in Fig. 3c & e for $\phi_b = 0.78$ and $d_0 = 15a$ where $d(t)$ decreases with time (see Supplementary Movie S1 and S2) in both experiment and simulation. This confirms our prediction of an attractive interaction mediated by activity and the elasticity of the crystalline medium of beads.

The motility of the rods is crucial for the attractive interaction. We have checked that apolar rods (of the same central diameter but symmetrically tapered at their ends) [56] show essentially no interaction when placed in the crystalline array of beads ([43], S8). This justifies our neglect, mentioned earlier, of direct couplings to elastic-

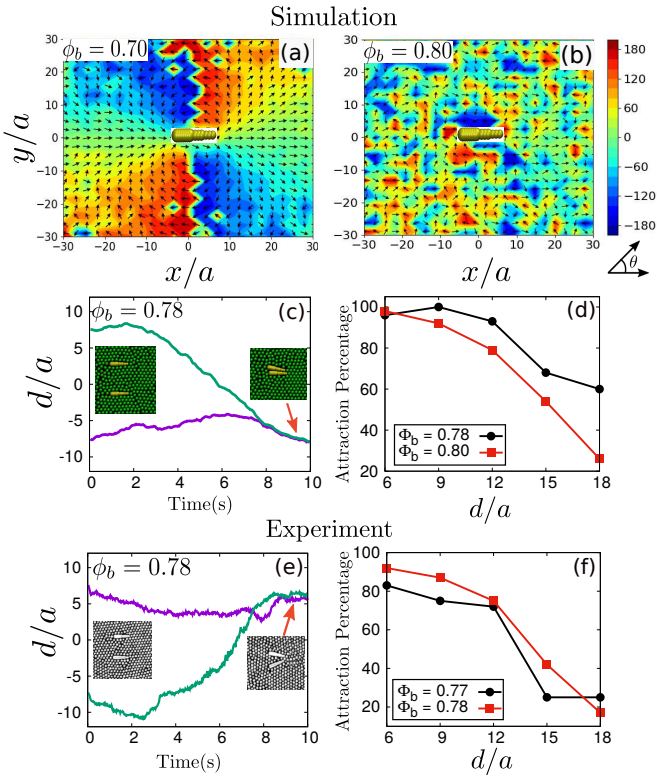


FIG. 3. Velocity field and elastic attraction: (a) and (b) show the unit vector plot of the velocity field around a single motile rod at bead area fraction $\phi_b = 0.70$, and $\phi_b = 0.80$. At $\phi_b = 0.70$, the flow pattern is similar to that predicted for a monopole force density [40, 55] in a fluid on a substrate, whereas at $\phi_b = 0.80$, the velocity field is suppressed due to the elastic behaviour of the medium. (e) & (g) show vertical coordinates of a pair of rods with initial separation $d_0 = 15a$ and $\phi_b = 0.78$ in experiment and simulation respectively, primary evidence for pair attraction in the crystalline medium. (f) Simulation & (h) experiment show that attraction probability P_a decreases with increasing initial separation for two values of ϕ_b .

ity in (1). Rotational noise in the rod dynamics in the experiments introduces a stochastic element in the capture process; particles occasionally turn away from each other and escape. To quantify the attraction between the rods in the presence of noise, for a given ϕ_b and d_0 , we have performed 50 (12) independent runs in the simulation (experiment). We then calculate the percentage P_a of trajectories for which the lateral distance between the rods goes below 5 bead radii after travelling around 80 bead radii in the longitudinal direction. Non-interacting rods, as a result of rotational noise, would turn towards or away from each other with equal probability, so P_a would be 50 %. We therefore use $P_a > 50\%$ as a reasonable statistical definition of attraction. Fig. 3d & f present P_a vs initial separation in experiment and simulation. A substantial decline with increasing d_0 at fixed

ϕ_b is clearly seen. A perceptible decrease in P_a as ϕ_b is increased from 0.78 to 0.80 in the simulation is probably because the lattice is beginning to jam, thus suppressing the strain field required for attraction.

It is clear from the formulation (4)-(7) that the interaction between the motile particles is a consequence of the reorientation of their active motion rather than a pair potential. We now underline the nonequilibrium character of this interaction by a direct demonstration of its non-reciprocal nature. Unlike in [30, 31, 35], we are dealing here with interactions between two particles of the same type, so non-reciprocity operates with respect to their relative locations and orientations, as in [28, 29, 32–34]. The strain field generated by each motile rod reorients the other, thus redirecting their velocities. The fore-aft asymmetry of the lattice distortion in (5) and Fig. 1 implies that if one rod is situated in front of another, as defined by the heading of the latter, the two experience drastically different reorienting torques. The strain field generated ahead of the trailing rod is highly screened, unlike that which the leading rod produces in its wake. We expect the trailing rod to reorient strongly, while effectively concealing its approach from the leading rod. We illustrate this through theoretically calculated particle trajectories which we compare with laboratory and numerical experiments.

We consider a pair of particles initially aligned perpendicular to each other, pointing along say the x and y directions. We isolate the key role of the apolar coupling κ in (7) by setting $\gamma_1 = \gamma_2 = 0$, and show that for $\kappa > 0$ capture always takes place, as illustrated in Fig. 4a for $\kappa f/\mu v_0 = 100$. The calculated dynamics graphically reiterates what we argued qualitatively above: the encounter takes place by one particle approaching the other from behind, and turning towards it, while the particle in front moves entirely oblivious of the approach of the other, see Fig. 4a, a direct consequence of the strong fore-aft asymmetry in the screening of the displacement fields of the moving particles, (5). We find convincing confirmation of this prediction in our simulation as well as in experiment, see Fig. 4b & c and Supplementary Movie S9, S10.

Lastly there is the question of the relative importance of the polar and apolar couplings in (7). The streamline plots, Fig. 2, suggest that γ_1, γ_2 give rise to more complex and rapid spatial variation than the apolar strain-aligning κ term and do not play an important role in the pair attraction. We illustrate these distinct roles by plotting trajectories calculated by numerically solving (7) and (1) for the pair, with $\kappa = 0$, for various positive and negative values of γ_1, γ_2 , and see that in all cases capture does not take place. We also show that for $\gamma_1, \gamma_2 = \pm 10$ and $\kappa < 0$ again capture is unsuccessful (Supplementary Fig. 6 [43]). The reason is that the alignment directions of the rods would now have to be perpendicular to those shown in Fig. 2b.

In conclusion, we have constructed the theory of the

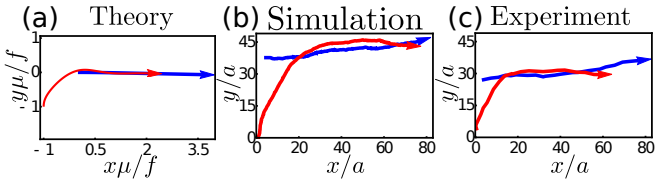


FIG. 4. Nonreciprocity in capture. Trajectories of two polar particles which are initially pointing normal to each other. (a) in theory for $\gamma_1/v_0 = \gamma_2/v_0 = 0$ and $\kappa f/\mu v_0 = 100$, (b) in simulation and (c) in experiment at $\phi_b = 0.78$ for initial y separation $39.4a$ and $26a$ respectively.

dynamics of active particles moving through an elastic medium on a substrate, and show that they interact by reorienting each other via elastic distortions created by their motility. The result is a non-potential, non-reciprocal sensing and trail-following behaviour of purely mechanical origin. Through experiments in the laboratory and on the computer, on macroscopic particles rendered active by mechanical vibration, we have confirmed the predicted form of the elastic disturbances and the non-reciprocal attraction and pursuit. This interaction should be observed between motile cells in a supported gel layer or epithelium, and possibly in chase-and-run dynamics in cell migration [57, 58]. Modifications associated with momentum conservation arise in principle for a bulk 3-dimensional medium such as the extracellular matrix but even there the relatively rigid components of the matrix could serve, over some time- and length-scales, as a momentum sink for the dynamics of the more deformable components. Multiparticle behaviour, the competition between alignment and attraction in the collective dynamics, and the effect of quenched disorder, as well as the relation between the parameters of our coarse-grained theory and particle-scale properties remain outstanding challenges.

RKG thanks the Department of Physics, Indian Institute of Science, for hospitality and support. RK was supported by the University Grants Commission, AKS by a Year of Science Professorship from the DST, HS by the SERB, and SR by a J C Bose Fellowship from the SERB and a Homi Bhabha Chair Professorship from the Tata Education & Development Trust. SR thanks E Tjhung and M Cates for discussions, and DAMTP, Cambridge for support and hospitality, funded in part by the European Research Council under the EU's Horizon 2020 Programme, Grant number 740269. SR and AKS acknowledge illuminating discussions during the KITP 2020 online program on Symmetry, Thermodynamics and Topology in Active Matter. This research was supported in part by the National Science Foundation under Grant No. NSF PHY-1748958.

- [1] C. M. Pooley, G. P. Alexander, and J. M. Yeomans, *Phys. Rev. Lett.* **99**, 228103 (2007).
- [2] A. Baskaran and M. C. Marchetti, *Proceedings of the National Academy of Sciences* **106**, 15567 (2009).
- [3] M. C. Marchetti, J. F. Joanny, S. Ramaswamy, T. B. Liverpool, J. Prost, M. Rao, and R. A. Simha, *Rev. Mod. Phys.* **85**, 1143 (2013).
- [4] D. Saintillan and M. J. Shelley, in *Complex Fluids in biological systems* (Springer, 2015) pp. 319–355.
- [5] J. Elgeti, R. G. Winkler, and G. Gompper, *Reports on progress in physics* **78**, 056601 (2015).
- [6] J. D. Eshelby, *Proceedings of the Royal Society of London. Series A.*
- [7] A. Ajdari, B. Duplantier, D. Hone, L. Peliti, and J. Prost, *Journal de Physique II* **2**, 487 (1992).
- [8] R. Golestanian, M. Goulian, and M. Kardar, *Physical Review E* **54**, 6725 (1996).
- [9] S. Katira, K. K. Mandadapu, S. Vaikuntanathan, B. Smit, and D. Chandler, *eLife* **5**, e13150 (2016).
- [10] D. Bartolo, A. Ajdari, and J.-B. Fournier, *Physical Review E* **67**, 061112 (2003).
- [11] O. Granek, Y. Baek, Y. Kafri, and A. P. Solon, *Journal of Statistical Mechanics: Theory and Experiment* **2020**, 063
- [12] U. S. Schwarz and S. A. Safran, *Phys. Rev. Lett.* **88**, 048102 (2002).
- [13] I. B. Bischofs, S. A. Safran, and U. S. Schwarz, *Phys. Rev. E* **69**, 021911 (2004).
- [14] J. Yuval and S. A. Safran, *Phys. Rev. E* **87**, 042703 (2013).
- [15] O. Cohen and S. A. Safran, *Soft Matter* **12**, 6088 (2016).
- [16] R. Golkov and Y. Shokef, *New Journal of Physics* **19**, 063011 (2017).
- [17] R. Golkov and Y. Shokef, *Physical Review E* **99**, 032418 (2019).
- [18] P. Marcq, *The European Physical Journal E* **37**, 29 (2014).
- [19] S. Banerjee and M. C. Marchetti, *EPL (Europhysics Letters)* **96**, 28003 (2011).
- [20] S. Banerjee, K. J. Utuji, and M. C. Marchetti, *Physical Review Letters* **114**, 228101 (2015).
- [21] M. Köpf and L. Pismen, *Physica D: Nonlinear Phenomena* **259**, 48 (2013).
- [22] J. Notbohm, S. Banerjee, K. J. Utuji, B. Gweon, H. Jang, Y. Park, J. Shin, J. P. Butler, J. J. Fredberg, and M. C. Marchetti, *Biophysical Journal* **110**, 2729 (2016).
- [23] F. Alaimo, S. Praetorius, and A. Voigt, *New Journal of Physics* **18**, 083008 (2016).
- [24] A. M. Menzel and H. Löwen, *Physical Review Letters* **110**, 055702 (2013).
- [25] A. Maitra and S. Ramaswamy, *Physical Review Letters* **123**, 238001 (2019).
- [26] S. Henkes, K. Kostanjevec, J. M. Collinson, R. Sknepnek, and E. Bertin, *Nature communications* **11**, 1405 (2020).
- [27] However, for the present approach to apply in detail the 3D system would have to be everywhere in contact with a momentum sink such as a porous medium.
- [28] J. Das, M. Rao, and S. Ramaswamy, *EPL (Europhysics Letters)* **60**, 418 (2002).
- [29] J. Das, M. Rao, and S. Ramaswamy, *arXiv:cond-mat/0404071* (2004).
- [30] A. Ilev, J. Bartnick, M. Heinen, C.-R. Du, V. Nosenko, and H. Löwen, *Physical Review X* **5**, 011035 (2015).

[31] A. Cavagna, I. Giardina, A. Jelic, S. Melillo, L. Parisi, E. Silvestri, and M. Viale, *Physical Review Letters* **118**, 138003 (2017).

[32] Q.-s. Chen, A. Patelli, H. Chaté, Y.-q. Ma, and X.-q. Shi, *Physical Review E* **96**, 020601(R) (2017).

[33] S. Saha, S. Ramaswamy, and R. Golestanian, *New Journal of Physics* **21**, 063006 (2019).

[34] L. P. Dadhichi, J. Kethapelli, R. Chajwa, S. Ramaswamy, and A. Maitra, *Physical Review E* **101**, 052601 (2020).

[35] M. Fruchart, R. Hanai, P. B. Littlewood, and V. Vitelli, *arXiv:2003.13176* (2020).

[36] S. Saha, J. Agudo-Canalejo, and R. Golestanian, *arXiv:2005.07101* (2020).

[37] Z. You, A. Baskaran, and M. C. Marchetti, *arXiv:2005.07684* (2020).

[38] L. D. Landau, E. M. Lifshitz, A. M. Kosevich, and L. P. Pitaevskii, *Theory of Elasticity*, 3rd ed. (Butterworth-Heinemann, 1986).

[39] This would appear in the form of a coupling of \mathbf{n} to an anisotropic potential with the point-group symmetry of the lattice.

[40] N. Kumar, H. Soni, S. Ramaswamy, and A. K. Sood, *Nat Commun* **5**, 4688 (2014).

[41] I. S. Aranson, A. Sokolov, J. O. Kessler, and R. E. Goldstein, *Physical Review E* **75**, 040901 (2007).

[42] A. Maitra, P. Srivastava, M. C. Marchetti, S. Ramaswamy, and M. Lenz, *Physical Review Letters* **124**, 028002 (2020).

[43] See Supplementary Information below and Supplementary videos at <https://www.dropbox.com/sh/od5lg00cxijk7b9/AAB3j6e17j8a10qMay01q2A?d=1>.

[44] I. S. Gradshteyn and I. M. Ryzhik, *Table of integrals, series, and products* (Academic press, 2014).

[45] At large wavevectors \mathbf{q} where the v_0 term can be ignored, the Fourier transform $\mathbf{U}_\mathbf{q} \sim f/\mu q^2$, i.e., f/μ as a source for the displacement field enters in a manner reminiscent of the Burgers vector of a dislocation.

[46] S. Saha, R. Golestanian, and S. Ramaswamy, *Physical Review E* **89**, 062316 (2014).

[47] A. Zöttl and H. Stark, *Journal of Physics: Condensed Matter* **28**, 253001 (2016).

[48] B. Liebchen, D. Marenduzzo, and M. E. Cates, *Physical Review Letters* **118**, 268001 (2017).

[49] R. Golestanian, *arXiv:1909.03747* (2019).

[50] O. Peleg, J. M. Peters, M. K. Salcedo, and L. Mahadevan, *Nature Physics* **14**, 1193 (2018).

[51] N. Yoshinaga, J.-F. Joanny, J. Prost, and P. Marcq, *Physical Review Letters* **105**, 238103 (2010).

[52] N. Kumar, R. K. Gupta, H. Soni, S. Ramaswamy, and A. K. Sood, *Phys. Rev. E* **99**, 032605 (2019).

[53] H. Soni, N. Kumar, J. Nambisan, R. K. Gupta, A. K. Sood, and S. Ramaswamy, *Soft Matter*, (2020).

[54] N. Kumar, H. Soni, S. Ramaswamy, and A. K. Sood, *Phys. Rev. E* **91**, 030102 (2015).

[55] T. Brotto, J.-B. Caussin, E. Lauga, and D. Bartolo, *Phys. Rev. Lett.* **110**, 038101 (2013).

[56] V. Narayan, S. Ramaswamy, and N. Menon, *Science* **317**, 105 (2007), <http://www.sciencemag.org/content/317/5834/105.full.pdf>.

[57] E. Theveneau, B. Steventon, E. Scarpa, S. García, X. Trepaut, A. Streit, and R. Mayor, *Nature cell biology* **15**, 763 (2013).

[58] R. Mayor, B. Steventon, M. Das, and J. M. Schwarz, *Physical Review E* **96**, 032407 (2017).

Supplementary Information

Rahul Kumar Gupta¹, Raushan Kant², Harsh Soni², A.K. Sood² and Sriram Ramaswamy²

¹*Tata Institute of Fundamental Research,*

Gopanpally, Hyderabad 500 107 India and

²*Department of Physics, Indian Institute of Science, Bangalore 560 012, India*

(Dated: August 10, 2020)

S1. DETAILED THEORY

Displacement field around a motile particle

As discussed in the main text, we assume that the motile particle oriented along $\mathbf{n}(t)$ exerts a force monopole density $f\delta(\mathbf{r} - \mathbf{R}(t))\mathbf{n}(t)$ on the elastic medium, where $\mathbf{R}(t)$ is the position of the motile particle. Then the equation of motion for the displacement field \mathbf{u} for the elastic medium on a substrate is given by

$$\zeta\partial_t\mathbf{u} = -\frac{\delta F}{\delta\mathbf{u}} + f\delta(\mathbf{r} - \mathbf{R}(t))\mathbf{n}(t), \quad (1)$$

where F is the free energy functional for the elastic medium and ζ is the dissipation constant of the substrate.

Assuming that the dynamics of elastic medium is governed by the free energy functional $F = \int d^2x [\lambda(\text{Tr}\boldsymbol{\varepsilon})^2/2 + \mu\text{Tr}(\boldsymbol{\varepsilon}^2)]$ [1], Eq. (1) becomes

$$\zeta\partial_t\mathbf{u} = (\mu\nabla^2 + \lambda\boldsymbol{\nabla}\boldsymbol{\nabla}\cdot)\mathbf{u} + f\delta(\mathbf{r} - \mathbf{R}(t))\mathbf{n}(t). \quad (2)$$

For simplicity, we consider that the motile particle moves with a constant speed v_0 along $\mathbf{n}(t)$. Therefore,

$$\dot{\mathbf{R}}(t) = v_0\mathbf{n}(t). \quad (3)$$

Let $\mathbf{U}(\mathbf{r}', t)$ be the displacement field in a coordinate frame S comoving and co-rotating with the motile particle and \mathbf{S} is the rotation matrix from frame S to the lab frame then $\mathbf{u}(\mathbf{r}, t) = \mathbf{S}(t) \cdot \mathbf{U}(\mathbf{r}', t)$, where $\mathbf{r}' = \mathbf{S}^T \cdot (\mathbf{r} - \mathbf{R}(t))$. Considering that the motile particle is oriented along the x direction in frame S, $\mathbf{n}(t) = \mathbf{S}(t) \cdot \hat{\mathbf{x}}$. Then, from Eq. (2)

$$\zeta \left[\frac{\partial}{\partial t} + \mathbf{S}^T \cdot \dot{\mathbf{S}} \cdot + \mathbf{r}' \cdot \mathbf{S}^T \cdot \dot{\mathbf{S}} \cdot \boldsymbol{\nabla}' \right] \mathbf{U} = [\zeta v_0 \partial'_x + (\mu\nabla'^2 + \lambda\boldsymbol{\nabla}'\boldsymbol{\nabla}'\cdot)]\mathbf{U} + f\delta(\mathbf{S} \cdot \mathbf{r}')\hat{\mathbf{x}}. \quad (4)$$

For the motile particle pointing at angle $\theta(t)$ from the x axis, $\mathbf{n}(t) = (\cos\theta(t), \sin\theta(t))$ and the rotational matrix

$$\mathbf{S} = \begin{pmatrix} \cos\theta(t) & -\sin\theta(t) \\ \sin\theta(t) & \cos\theta(t) \end{pmatrix} \quad (5)$$

which gives us $\mathbf{S}^T \cdot \dot{\mathbf{S}} = \boldsymbol{\epsilon}^T \dot{\theta}$. Here $\boldsymbol{\epsilon}$ is the 2D Levi-Civita symbol. As $|\mathbf{S}| = 1$, $\delta(\mathbf{S} \cdot \mathbf{r}') = \delta(\mathbf{r}')$.

Then Eq. (4) reduces to

$$\zeta \left[\frac{\partial \mathbf{U}}{\partial t} + [\boldsymbol{\epsilon}^T \cdot \mathbf{U} + (\mathbf{r}' \cdot \boldsymbol{\epsilon}^T \cdot \boldsymbol{\nabla}')\mathbf{U}] \dot{\theta}(t) \right] = [\zeta v_0 \partial'_x + (\mu\nabla'^2 + \lambda\boldsymbol{\nabla}'\boldsymbol{\nabla}'\cdot)]\mathbf{U} + f\delta(\mathbf{r}')\hat{\mathbf{x}}. \quad (6)$$

For the motile particle subjected to no torque, $\dot{\theta}(t) = 0$ and \mathbf{U} will be constant in time in the stationary state *i.e.* $\mathbf{U} \equiv \mathbf{U}(\mathbf{r}')$ and the above equation is simplified to

$$[-\zeta v_0 \partial_x - (\mu \nabla^2 + \lambda \nabla \nabla \cdot)] \mathbf{U} = f \delta(\mathbf{r}) \hat{\mathbf{x}}. \quad (7)$$

Fourier transform of the above equation gives:

$$-iv_0 \zeta q_x \mathbf{U}_{\mathbf{q}} + \mu q^2 \mathbf{U}_{\mathbf{q}} + \lambda \mathbf{q} \mathbf{q} \cdot \mathbf{U}_{\mathbf{q}} = f \hat{\mathbf{x}}, \quad (8)$$

where $\mathbf{U}_{\mathbf{q}}$ is the Fourier transform of \mathbf{U} . Solving above equation for $\mathbf{U}_{\mathbf{q}}$, we obtain:

$$\begin{aligned} \mathbf{U}_{\mathbf{q}} = & \left(\frac{f \xi}{\mu(\xi q^2 - iq_x)} + \frac{f q_x \xi}{i \zeta v_0 (q^2 \xi - iq_x \nu)} - \frac{f q_x \xi}{i \zeta v_0 (q^2 \xi - iq_x)} \right) \hat{\mathbf{x}} \\ & + \left(\frac{if q_y \xi}{i \zeta v_0 (\xi q^2 - iq_x \nu)} - \frac{if q_y \xi}{i \zeta v_0 (q^2 \xi - iq_x)} \right) \hat{\mathbf{y}}, \end{aligned} \quad (9)$$

where $\xi = \mu/\zeta v_0$ and $\nu = (1 + \eta^{-1})$ with $\eta = \lambda/\mu$. Now, to derive the expression of \mathbf{U} , we first perform the inverse Fourier transform of $\mathbf{U}_{\mathbf{q}}$ with respect to q_x using the contour integration, and then with respect to q_y using already solved integrals given in [2]. It gives us the following expressions of x - and y -component of \mathbf{U} :

$$\begin{aligned} U_x &= \frac{f}{4\pi\mu} \left[\left[K_0\left(\frac{r}{2\xi}\right) - \frac{x}{r} K_1\left(\frac{r}{2\xi}\right) \right] e^{-\frac{x}{2\xi}} + \nu \left[K_0\left(\frac{r\nu}{2\xi}\right) + \frac{x}{r} K_1\left(\frac{r\nu}{2\xi}\right) \right] e^{-\frac{x\nu}{2\xi}} \right] \\ U_y &= \frac{f}{4\pi\mu r} y \left[\nu K_1\left(\frac{r\nu}{2\xi}\right) e^{-\frac{x\nu}{2\xi}} - K_1\left(\frac{r}{2\xi}\right) e^{-\frac{x}{2\xi}} \right], \end{aligned} \quad (10)$$

where $r = \sqrt{x^2 + y^2}$ and K_0 and K_1 are the modified Bessel functions of the second kind.

Coupled dynamics of two motile particles in elastic medium

Let us consider two motile particles whose orientations and positions at time t are denoted by $\mathbf{n}_i(t) \equiv (\cos \theta_i(t), \sin \theta_i(t))$ and $\mathbf{R}_i(t)$ ($i = 1, 2$), respectively. Then the displacement field in the lab frame created by i th particle will be

$$\mathbf{u}_i(\mathbf{r}, t) = \mathbf{S}_i(t) \cdot \mathbf{U}_i(\mathbf{r}'_i, t) \quad (11)$$

with

$$\mathbf{r}'_i(t) = \mathbf{S}_i(t)^T \cdot (\mathbf{r} - \mathbf{R}_i(t)), \quad (12)$$

where the rotation matrix $\mathbf{S}_i(t)$ is given by (see Eq.(6)):

$$\mathbf{S}_i(t) = \begin{pmatrix} \cos \theta_i(t) & -\sin \theta_i(t) \\ \sin \theta_i(t) & \cos \theta_i(t) \end{pmatrix}. \quad (13)$$

The displacement field $\mathbf{U}_i(\mathbf{r}, t)$ due to i th motile particle in its comoving and co-rotating frame follows the equation of motion (see Eq. (6)):

$$\zeta \left[\frac{\partial \mathbf{U}_i}{\partial t} + [\boldsymbol{\epsilon}^T \cdot \mathbf{U}_i + (\mathbf{r} \cdot \boldsymbol{\epsilon}^T \cdot \boldsymbol{\nabla}) \mathbf{U}_i] \dot{\theta}_i(t) \right] = [\zeta v_0 \partial_x + (\mu \nabla^2 + \lambda \boldsymbol{\nabla} \boldsymbol{\nabla} \cdot)] \mathbf{U}_i + f \delta(\mathbf{r}) \hat{\mathbf{x}}. \quad (14)$$

We now assume that the motile particles mutually interact with each other via their displacement fields $\mathbf{u}_i(\mathbf{r}, t)$. As argued in the main text, the dynamics of the orientation of i th particle is governed by the equation of motion:

$$\frac{d\mathbf{n}_i(t)}{dt} = (\mathbf{I} - \mathbf{n}_i \mathbf{n}_i) \cdot (\gamma_1 \nabla^2 \mathbf{u}_j + \gamma_2 \boldsymbol{\nabla} \boldsymbol{\nabla} \cdot \mathbf{u}_j + \kappa \boldsymbol{\varepsilon}_j \cdot \mathbf{n}_i), \quad (15)$$

where $\boldsymbol{\varepsilon}_j$ is the traceless part of the strain tensor $(\boldsymbol{\nabla} \mathbf{u}_j + \boldsymbol{\nabla} \mathbf{u}_j^T)/2$ and $j = 1(2)$ for $i = 2(1)$.

We can easily see from the above equation that equation of motion for $\dot{\theta}_i$ will be

$$\dot{\theta}_i(t) = \hat{\mathbf{z}} \cdot [\mathbf{n}_i \times (\gamma_1 \nabla^2 \mathbf{u}_j + \gamma_2 \boldsymbol{\nabla} \boldsymbol{\nabla} \cdot \mathbf{u}_j + \kappa \boldsymbol{\varepsilon}_j \cdot \mathbf{n}_i)]. \quad (16)$$

With the above expression of $\dot{\theta}_i$, the second term in the RHS of Eq.(14) will be a nonlinear term which we ignore in our calculation. Therefore, in the stationary state, the displacement field \mathbf{U}_i is simply given by Eq.(10).

From Eq. (3), the position $\mathbf{R}_i(t)$ of i th particle obeys

$$\dot{\mathbf{R}}_i(t) = v_0 \mathbf{n}_i(t). \quad (17)$$

We integrate Eqs (15) and (17) numerically to get the trajectories of the two particles in the elastic medium.

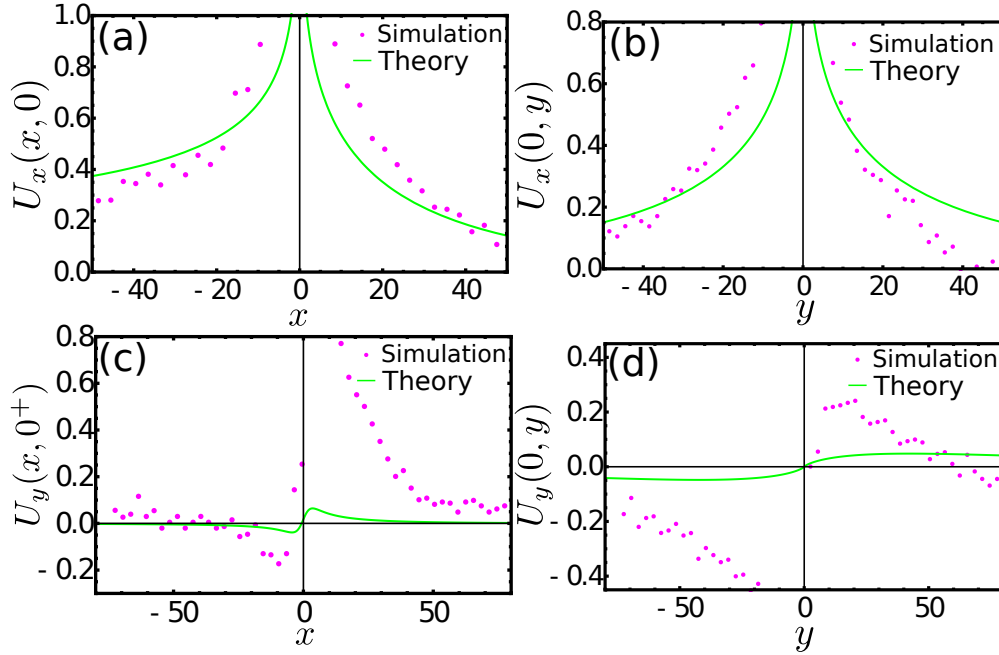
S2. ON THE COUPLING OF ROD ORIENTATION TO STRAIN

The particles in the experiments and simulations are rods tapered towards one tip, and self-propel with the tapered end forward. Considerations of excluded volume suggest that the fat, i.e., non-tapered end would be more easily accommodated in dilated regions, and on the “outside” of a curved region of crystal. This suggests that \mathbf{n} would like to point antiparallel to $\nabla\nabla \cdot \mathbf{u}$ but parallel to $\nabla^2\mathbf{u}$, i.e., $\gamma_1 > 0, \gamma_2 < 0$. However, the interactions could be kinetic in which case essentially entropic excluded-volume arguments are not a good guide. A sensory or behavioral motility-strain coupling arises in a recent model of honeybee swarm mechanics [3], in which bees orient and move towards regions of large dilation, which would amount to $\gamma_2 > 0$.

S3. INFERRING THE DISPLACEMENT FIELD FROM THE PARTICLE SIMULATION

In order to extract the displacement field, we first evaluate the time-averaged number density profile of the beads $\rho(\mathbf{r})$ around a moving rod in its rest frame. We then determine the positions of peaks of the $\rho(\mathbf{r})$ field, which gives us a distorted lattice $\rho_d(\mathbf{r})$ corresponding to the deformed crystalline bead medium. It is clear from our observations that far away from the rod, the lattice remains undistorted. Hence, we construct the ideal lattice $\rho_0(\mathbf{r})$ by extrapolating the lattice profile far away from the rod. The change in the position of a given lattice point as we go from the ideal lattice to the distorted lattice gives us the displacement $\mathbf{u}_e(\mathbf{r})$ at the position of the lattice point \mathbf{r} in the ideal lattice. We now calculate the displacement field $\mathbf{u}_e(\mathbf{r})$ by mapping $\rho_d(\mathbf{r})$ onto $\rho_0(\mathbf{r})$ as $\rho_0(\mathbf{r}) = \rho_d(\mathbf{r} + \mathbf{u}_e(\mathbf{r}))$.

S4. FITTING THE NUMERICAL DISPLACEMENT FIELD TO THE THEORY



Supplementary Figure 1. The displacement field components U_x and U_y as the function of x and y as observed in the simulation (dots) and corresponding theoretical fits (line). (a) U_x vs x at $y = 0$. (b) U_x vs y at $x = 0$. (c) U_y vs x at $y = 4a$. (d) U_y vs y at $x = 0$. Here the fitting parameters are calculating by fitting the x dependence of U_x at $y = 0$ and their values are $\eta = 1.3$, $f/\mu = 2.2a$ and $\alpha = 0.1$. The length unit is bead radius in the simulation.

We fit $U_x(x, y = 0)$ vs x calculated from the simulation at $\phi_b = 0.80$ to our theoretical model (see Eq. (10)) using least-squares method (see Fig. 1a). The values of fitting parameters are $\eta = 1.3$, $f/\mu = 2.2a$ and $\alpha = 0.1$. Fig. 1b shows that these parameter values provide a satisfactory fit to $U_x(x = 0, y)$ vs y as well (see Fig. 1b). However, the profile of U_y deviates from the theory with these parameter values (see Fig. 1c & d). We believe these departures arise because the thickness of the rod is larger than the bead diameter, and therefore the rod would distort the bead medium along the y direction even without the motility, giving rise to a purely static steric contribution to U_y with a jump at $y = 0$.

S5. EXPERIMENTAL AND SIMULATION DETAILS

Our experiments are performed with aluminium beads, diameter $D = 0.8$ mm and tapered brass rods, length $\ell = 4.5$ mm, with diameters 1.1 mm and 0.8 mm at the two ends, lying between a circular base plate of diameter 13 cm and a glass lid, separated by gap $w = 1.2$ mm [4–7], which is only a little more than the thick-end diameter of the rod, so the system forms a monolayer. The plate is mounted on a permanent-magnet shaker (LDS V406-PA 100E) driving it sinusoidally in the vertical direction with frequency $f = 200$ Hz and shaking strength $\Gamma \equiv \mathcal{A}(2\pi f)^2/g = 7.0$, where \mathcal{A} and g are the shaking amplitude and the gravitational acceleration, respectively. Images of the particles are recorded using a high-speed camera (Redlake MotionPro X3), which are further processed using ImageJ [8] to extract the trajectories of the particles. In numerical simulations, the rod is modelled as an array of overlapping spheres of different sizes [6] and the vertically vibrating plate and glass lid are represented by the two horizontal walls whose vertical positions at time t are given by $\mathcal{A} \cos 2\pi f t$ and $\mathcal{A} \cos 2\pi f t + w$, respectively. The particle-particle and particle-wall collisions are governed by the Impulse-based collision model [9] and the ballistic dynamics of the particles is governed by Newtonian rigid body dynamics. We use the time-driven particle dynamics algorithm to perform the simulations. VMD software [10] is used to make all the movies and snapshots from the simulations. The values of the friction and restitution coefficients are 0.05 and 0.3 for particle-particle collisions, 0.03 and 0.1 for rod-wall collisions, and 0.2 and 0.3 for bead-wall collisions, respectively. Periodic boundary conditions are applied in the xy plane to a square simulation box of side length $78a$.

S6. CHARACTERISTICS OF THE BEAD MEDIUM AT DIFFERENT ϕ_b

Hexatic order parameter and its correlation function

We examine here the ordering of the bead medium without rods [11], at varying bead area fraction ranging from 0.71 to 0.80. We focus on the global bond orientational order parameter ψ_6 and the bond orientational correlation function $g_B(r)$. We first evaluate the local orientational order parameter, defined as

$$\psi_{6,i} = \frac{1}{N_i} \sum_{j=1}^{N_i} \exp(6i\theta_{ij}), \quad (18)$$

where N_i is the number of particles within the cut-off distance r_{\min} from the i^{th} particle and θ_{ij} is the angle, with respect to a reference direction, made by the vector from the centre of the i^{th} to that of the j^{th} bead; r_{\min} is the position of the first minima of the radial distribution function

$$g(r) = \frac{1}{\rho_0} \langle \rho(\mathbf{r}') \rho(\mathbf{r}'') \rangle_{|\mathbf{r}' - \mathbf{r}''| = r}. \quad (19)$$

In the above expression, the angular bracket stands for the ensemble average over all values of \mathbf{r}' and \mathbf{r}'' with $|\mathbf{r}' - \mathbf{r}''| = r$ and,

$$\rho(\mathbf{r}) = \sum_{i=1}^N \delta(\mathbf{r} - \mathbf{r}_i) \quad (20)$$

is the number density field and ρ_0 is the average number density. We then calculate the global bond orientational order parameter

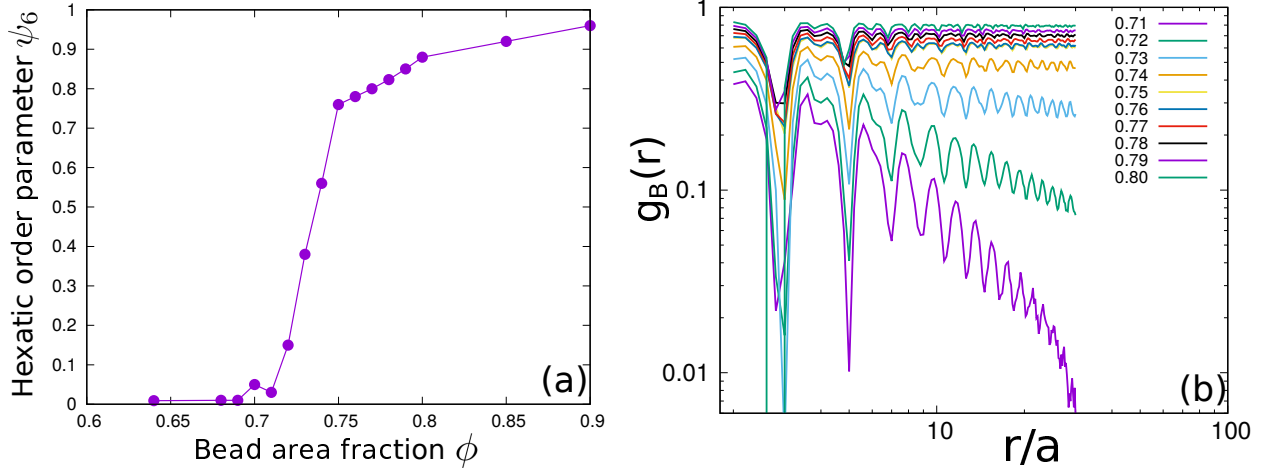
$$\psi_6 = \left| \sum_{i=1}^N \psi_{6,i} \right|. \quad (21)$$

Supplementary Fig. 1a shows the ψ_6 as a function of bead area fraction ϕ_b , ranging from 0.71 to 0.80. ψ_6 is close to zero below $\phi_b = 0.72$, implying that the bead medium lies in the liquid phase for $\phi_b < 0.72$, above $\phi_b = 0.72$, ψ_6 grows gradually with area fraction ϕ_b and saturates for $\phi_b > 0.78$.

We find that the behaviour of the bead monolayer as a function of area fraction is consistent with two-step melting [12]. The evidence for this comes from the the bond orientational correlation function

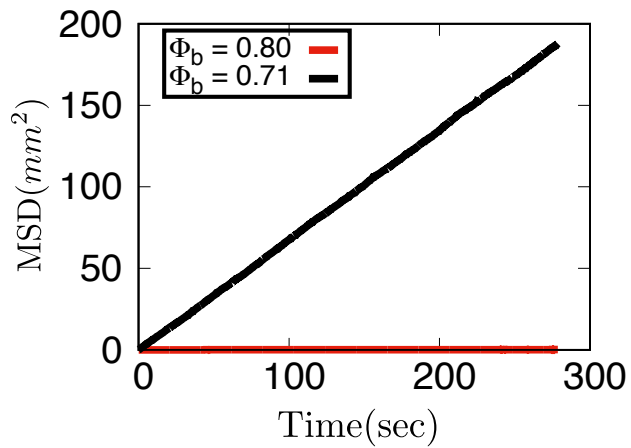
$$g_B(r) = \frac{\left\langle \psi_{6,i}^*(\mathbf{r}') \psi_{6,i}(\rho(\mathbf{r}'')) \right\rangle_{|\mathbf{r}' - \mathbf{r}''| = r}}{g(r)}.$$

Supplementary Fig. 1b shows that $g_B(r)$ decays exponentially with r for $\phi_b < 0.72$ and algebraically with r for $0.72 \leq \phi_b \leq 0.75$. For $\phi_b > 0.75$, $g_B(r)$ approaches a nonzero value for large r . This is consistent with the 2D melting scenario [12] in which the crystalline phase has long-range bond order (and quasi-long-range translational order), and the hexatic phase has quasi-long-range bond order. We can therefore use a nonzero hexatic order parameter as a reliable identifier of the crystalline phase.



Supplementary Figure 2. (a) ψ_6 order parameter as a function of bead area fraction ϕ_b . (b) Bond orientational correlation function vs distance r scaled by bead radius a at different values of ϕ_b .

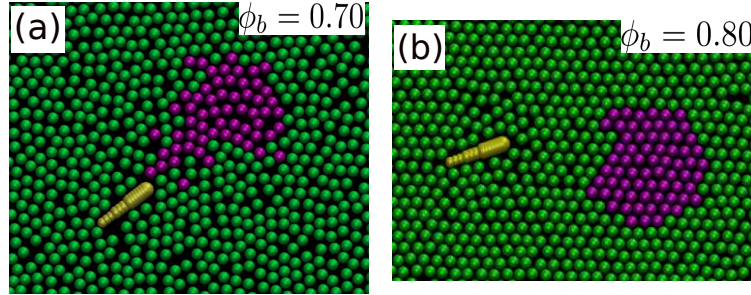
Mean squared displacement of the beads



Supplementary Figure 3. Mean squared displacement of the beads without rods at area fraction $\phi_b = 0.71$ and $\phi_b = 0.80$

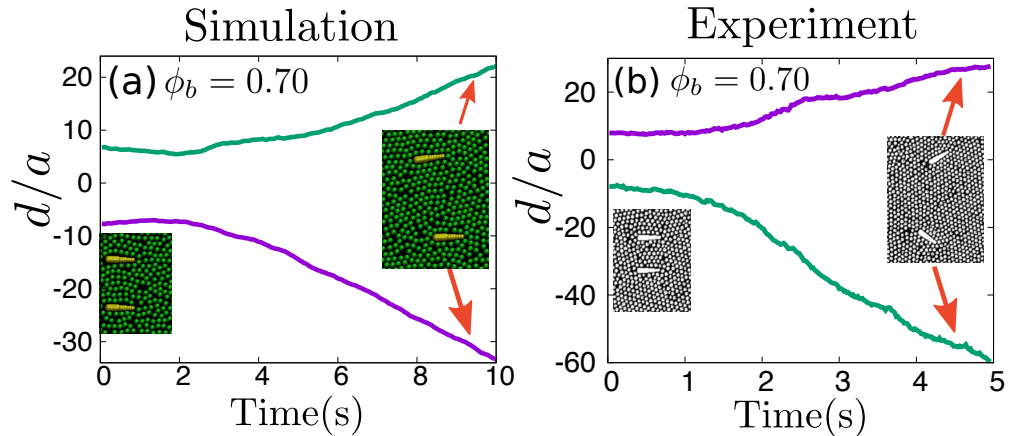
Motile rods drag beads in the fluid phase and not in the crystal

We see from Fig. 4b and Supplementary Movie 6 that the rod does not drag the beads around it at high ϕ_b , unlike the low ϕ_b ($=0.70$) case (Fig. 4a and Supplementary Movie 5). This observation is consistent with the crystalline character of the bead medium at high ϕ_b .



Supplementary Figure 4. (a) Dragging of surrounding beads (marked purple) by the rod due to their fluid-like state of organization at $\phi_b = 0.70$. (b) At $\phi_b = 0.80$, the beads around the rods remain almost unperturbed because of the crystalline nature of the bead medium.

S7. TWO-PARTICLE TRAJECTORIES IN FLUID MEDIUM



Supplementary Figure 5. Vertical coordinates of the particles with initial separation $d_0 = 15a$ and $\phi_b = 0.70$ in simulation (a) and in experiment (b).

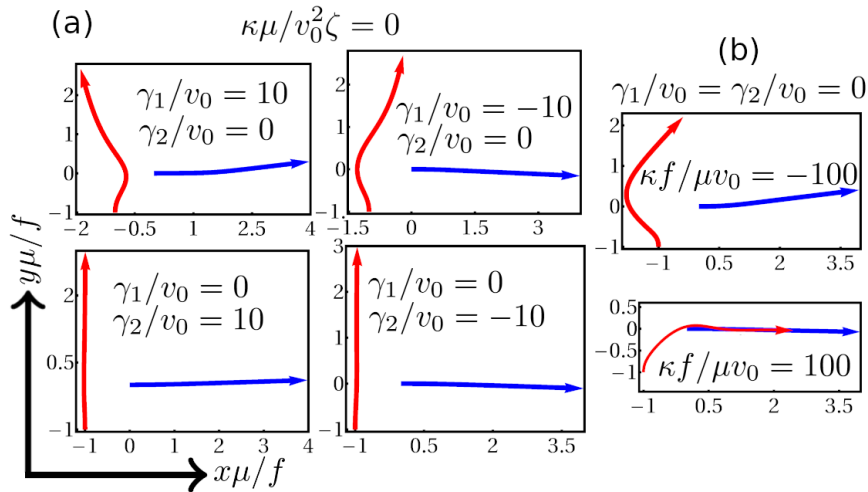
S8. MOTILITY MATTERS: APOLAR RODS DON'T ATTRACT

In the main article we discussed a variety of mechanisms that could give rise to interactions between inclusions in an ordered medium. Some operate in equilibrium systems [13–16], others in active systems [17], but none involved self-propelled motion. Here we show that such mechanisms are not at work in our system and that motility is essential for the attraction between active polar rods in our studies. We do this by examining the dy-

namics of two *apolar* rods, with the same central diameter as the polar rods of our study but tapered at both ends, suspended in the crystalline bead medium at area fraction $\phi_b = 0.70$ and $\phi_b = 0.80$. We find that the apolar rods neither attract nor repel each other (see Supplementary Movie 7 and 8). This observation shows unambiguously that motility is crucial for the attractive interaction of polar rods in our studies.

S9. PARTICLE TRAJECTORIES IN THEORY FOR DIFFERENT VALUES OF

γ_1, γ_2 AND κ



Supplementary Figure 6. Trajectories of two polar particles in theory which are initially pointing normal to each other, (a) for different values of γ_1/v_0 and γ_2/v_0 at $\kappa f/\mu v_0 = 0$, (b) for $\kappa f/\mu v_0 = -100$ and 100 at $\gamma_1/v_0 = \gamma_2/v_0 = 0$. Here $\alpha = 10$ and $\eta = 1$.

[1] L. D. Landau, E. M. Lifshitz, A. M. Kosevich, and L. P. Pitaevskii, *Theory of Elasticity*, 3rd ed. (Butterworth-Heinemann, 1986).

[2] I. S. Gradshteyn and I. M. Ryzhik, *Table of integrals, series, and products* (Academic press, 2014).

[3] O. Peleg, J. M. Peters, M. K. Salcedo, and L. Mahadevan, *Nature Physics* **14**, 1193 (2018).

[4] V. Narayan, S. Ramaswamy, and N. Menon, *Science* **317**, 105 (2007).

- [5] N. Kumar, S. Ramaswamy, and A. K. Sood, *Phys. Rev. Lett.* **106**, 118001 (2011).
- [6] N. Kumar, H. Soni, S. Ramaswamy, and A. K. Sood, *Nat Commun* **5**, 4688 (2014).
- [7] N. Kumar, H. Soni, S. Ramaswamy, and A. K. Sood, *Phys. Rev. E* **91**, 030102 (2015).
- [8] C. A. Schneider, W. S. Rasband, and K. W. Eliceiri, *Nature methods* **9**, 671 (2012).
- [9] W. J. Stronge, *Journal of Applied Mechanics* **61**, 605 (1994).
- [10] W. Humphrey, A. Dalke, and K. Schulten, *Journal of Molecular Graphics* **14**, 33 (1996).
- [11] J. Olafsen and J. Urbach, *Physical Review Letters* **95**, 098002 (2005).
- [12] B. I. Halperin and D. R. Nelson, *Phys. Rev. Lett.* **41**, 519 (1978).
- [13] J. D. Eshelby, *Proceedings of the Royal Society of London. Series A. Mathematical and physical sciences* **241**, 338 (1957).
- [14] A. Ajdari, B. Duplantier, D. Hone, L. Peliti, and J. Prost, *Journal de Physique II* **2**, 487 (1992).
- [15] R. Golestanian, M. Goulian, and M. Kardar, *Physical Review E* **54**, 6725 (1996).
- [16] S. Katira, K. K. Mandadapu, S. Vaikuntanathan, B. Smit, and D. Chandler, *eLife* **5**, e13150 (2016).
- [17] D. Bartolo, A. Ajdari, and J.-B. Fournier, *Physical Review E* **67**, 061112 (2003).